Bright phase-stable broadband fiber-based source of polarization-entangled photon pairs

J. Fan, M. D. Eisaman, and A. Migdall
Optical Technology Division, National Institute of Standards and Technology, 100 Bureau Drive, Mail Stop 8441, Gaithersburg, Maryland 20899-8441, USA
and Joint Quantum Institute, University of Maryland, College Park, Maryland 20742, USA
(Received 30 April 2007; revised manuscript received 27 June 2007; published 24 October 2007)

We describe an achromatic, phase-stable, broadband source of polarization-entangled photon pairs with high spectral brightness that uses four-wave mixing in a fiber Sagnac interferometer. We achieved a polarization-entangled two-photon coincidence rate of 7 kHz per 0.5 THz (0.9 nm) of bandwidth per 300 μW of average pump power. At this rate, we observed two-photon fringe interference visibilities greater than 97%, over a 10 THz ($\approx$21 nm) spectral range. We measured violations of Bell's inequality by more than 22 standard deviations for each of the four Bell states in less than 3 minutes per state. The high spectral brightness (26 kHz nm^{-1} mW^{-1}), large tunable wavelength range, single spatial mode, and phase stability make this source a promising candidate for a wide range of quantum-information applications.

DOI: 10.1103/PhysRevA.76.043836 PACS number(s): 42.65.Lm, 42.50.Dv, 03.65.Ud, 03.67.Hk

In recent years, fundamental and practical questions regarding quantum entanglement have led to fruitful research, ranging from tests of fundamental quantum-mechanical principles to quantum-information applications such as quantum nonlocality [1], quantum-key distribution [2], and quantum-state teleportation [3]. For example, it is now well known that two parties, each sharing half of an entangled photon pair, can use this entanglement to communicate with absolute security [4]. Despite the rapid progress over the last decade toward the practical application of these ideas, many challenges remain. In particular, for real-world quantum communication and cryptography applications to take advantage of entanglement, we need a robust source of entangled photon pairs with high spectral brightness, broad wavelength coverage, and a single-mode spatial output that is compatible with fiber networks or free-space operation.

Until recently, polarization-entangled photon-pair sources for such applications have been implemented almost exclusively using spontaneous parametric down-conversion in materials exhibiting $\chi^{(2)}$ optical nonlinearities. In this process, a pump photon at a frequency ω_P is converted into two lower-energy photons, satisfying energy conservation $\omega_P=\omega_1+\omega_2$ and the phase-matching condition $\vec{k}_P=\vec{k}_1+\vec{k}_2$ [5]. Because these conditions can be met over a wide range of parameters, photons are emitted into a large number of spatial and spectral modes, resulting in large collection losses when coupling into a single-mode optical fiber.

Recently, interest has shifted to materials exhibiting a third-order optical nonlinearity $\chi^{(3)}$, which allows, for example, spontaneous four-wave mixing (SFWM) to occur in single-mode optical fibers [6]. In such fibers, the centrosymmetry of the glass results in $\chi^{(2)}\approx 0$, with SFWM, the next-order process, becoming the dominant nonlinear wavelength conversion process. In SFWM, two photons are absorbed from the pump field (ω_P) to create a pair of correlated photons in a biphoton state satisfying $2\omega_P=\omega_s+\omega_i$, where the idler $\omega_i<\omega_P$ and the signal $\omega_s>\omega_P$. Two such biphoton states can be interferometrically combined together to form each of the four Bell states [7,8]. The advantage of a fiber-based source is obvious: polarization-entangled photon pairs can be created, selected, encoded, and delivered all within a single-mode fiber network with minimal losses.

In addition to the SFWM process that produces the biphoton states of interest, there is another competing nonlinear wavelength-conversion process that produces a broadband single-photon noise background—Raman scattering. In optical fibers, Raman scattering typically has a 40 THz bandwidth with a peak at 13 THz from the pump frequency [9]. In previous studies of fiber-based polarization-entangled two-photon sources, the wavelengths of the two-photon states were within the Raman spectral band [7,8], resulting in a quantum-interference fringe visibility as low as 30% at room temperature [8]. As a result, the fiber was cooled to liquid-nitrogen temperatures to significantly deplete the phonon population in the fiber. This, in turn, reduced the contribution of Raman scattering, and therefore improved the two-photon quantum-interference fringe visibility to a value of 97% [10]. While cooling improves the visibility, the two-photon coincidence rate of $\approx$100 Hz and limited spectral range [11] made the overall performance demonstrated in these previous experiments far below that of a typical spontaneous parametric down-conversion source.

In this paper, we report the development of a polarization-entangled photon-pair source, based on a polarization-configured fiber Sagnac interferometer, that addresses many of the drawbacks of previous sources. Operating at room temperature and bidirectionally pumping this Sagnac interferometer with a total average pump power of 300 μW, we measured a two-photon coincidence rate of 7 kHz for 0.5 THz (0.9 nm) bandwidth. The measured quantum-interference fringe visibilities are greater than 91% for raw coincidence counts uncorrected for background and 97% after subtracting accidental coincidences. In less than 3 minutes per Bell state, we completed measurements testing Bell's inequality in the Clauser-Horne-Shimony-Holt form [12], demonstrating a violation of the classical limit by more than 22 standard deviations for each of the four Bell states. The wavelength of the polarization-entangled two-photon state produced by our source can be chosen anywhere in a 10 THz ($\approx$21 nm) range. This source, with its single-spatial-

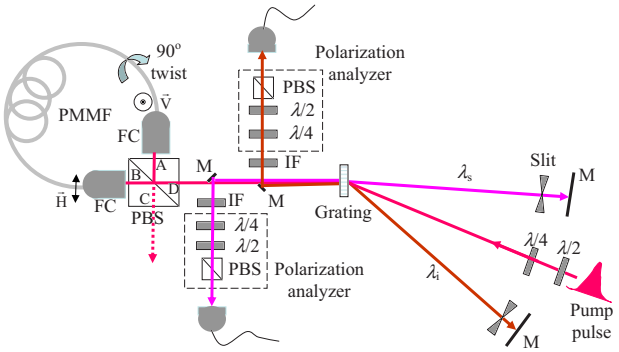

FIG. 1. (Color online) Schematic of the experimental setup. PMMF, polarization-maintaining microstructure fiber; FC, fiber coupler; PBS, polarizing beam splitter; λ/2, half-wave plate; λ/4, quarter-wave plate; M, mirror; IF, interference filter.

mode output, high spectral brightness, large available spectral bandwidth, and phase stability, is suitable for a wide range of practical quantum-information applications.

The experimental setup is shown in Fig. 1. After passing through a transmission grating, the 8 ps pump laser pulse (λ_P=740.7 nm, repetition rate of 80 MHz) is incident onto a polarizing beam splitter (PBS), splitting into a horizontally (H) polarized pump pulse (exiting port B of PBS) and a vertically (V) polarized pump pulse (exiting port A of PBS). A 1.8-m-long polarization-maintaining microstructure fiber (PMMF, zero-dispersion wavelength λ_{ZDW}=745±5 nm, nonlinearity γ=70 W^{-1} km^{-1} at λ_P) is arranged with its principal axis oriented horizontally at one end to accept (or output) the H-polarized light beam from (or to) port B and oriented vertically at the other end to accept (or output) the V-polarized light beam from (or to) port A. The PMMF and the PBS form a polarization-configured fiber Sagnac interferometer. With the small spatial-mode size of the microstructure fiber made possible by the large index difference between the glass core and air cladding [13], and the resulting high optical intensities, the PMMF exhibits high SFWM gain at large detuning from the pump wavelength where the Raman gain is lower. (For a detailed discussion of design and engineering of microstructure fiber, see Refs. [14,15].) The PMMF has the additional property that it maintains a single spatial mode for all wavelengths coupled in along its principal axis, as well as maintaining a single polarization mode. The polarization extinction ratio of the fiber Sagnac interferometer is measured to be better than 300:1.

The two pump pulses counterpropagate along the same principal axis in the PMMF. The biphoton states produced through SFWM by the H-polarized pump pulse, which is coupled into the PMMF through port B of the PBS, are output via port A in the V-polarization state $[V_s(\omega)V_i(-\omega)$, where ω is the frequency detuning from the pump wavelength, $\omega=\omega_s-\omega_P=\omega_P-\omega_i]$. The biphoton states produced by the V-polarized pump pulse, which is coupled into the PMMF through port A of the PBS, are output via port B in the H-polarization state $[H_s(\omega)H_i(-\omega)]$. These two SFWM processes, driven by equal-power counterpropagating laser pulses, produce equal outputs. Upon exiting, the cross-polarized biphoton states coherently overlap at the PBS to produce polarization-entangled Bell states in the form $\Phi^+(\omega)=H_s(\omega)H_i(-\omega)+V_s(\omega)V_i(-\omega)$.

With a two-pass grating configuration [16], the Bell state $\Phi^+=H_sH_i+V_sV_i$ (ω is dropped for simplicity), at a particular frequency with a collection bandwidth of $\Delta\omega$=0.5 THz (0.9 nm), is selected simply by moving the slits shown in Fig. 1 to a pair of positions to select conjugate signal and idler wavelengths that are connected by energy conservation. The use of the two-pass grating configuration not only maintains the selected photons in single spatial modes, but also provides better spectral rejection of other wavelengths. The other three Bell states are created by appropriate orientations of the quarter (λ/4) and half (λ/2) wave plates in the pump, and/or in the signal (or the idler) beam paths. The Bell states produced are measured using a polarization analyzer and single-photon detector (Si avalanche photodiode) in the signal and idler beam paths. The detector signals are sent to a logic circuit to count the coincidences and accidental coincidences. Each polarization analyzer consists of, in order, a λ/4-wave plate, a λ/2-wave plate, and a PBS.

The Bell state $\Phi^+=H_sH_i+V_sV_i$ created at the PBS passes through many optical elements before entering the polarization analyzer. In practice, the transmission efficiency of an optical element is less than unity and can vary with wavelength and polarization. Assuming more loss of V-polarized than H-polarized photons during propagation, the entangled quantum state becomes $\chi=H_sH_i+cV_sV_i$ with $c<1$, when it enters the analyzer. To eliminate this polarization imbalance, one can actively introduce more loss to H-polarized photons to equalize the amplitudes for the H_sH_i and V_sV_i terms. Instead of using this method, we rotate the polarization of the pump pulse to increase the relative probability of producing a V-polarized biphoton state. The use of unequal pump power for the two pump pulses also produces different self-phase-modulation (of the pump pulse) and cross-phase-modulation (induced by the pump pulse in the created photons) in the two nonlinear processes in the PMMF [9], yielding a relative phase difference 2φ between the two created biphoton states H_sH_i and V_sV_i. Thus the quantum state at the PBS is $\chi=H_sH_i+(1/c)e^{i2\varphi}V_sV_i$. After passing through various optical elements to enter the polarization analyzers, the state becomes $\chi=H_sH_i+e^{i2\varphi}V_sV_i$. Here, the system-induced relative phase difference between the two biphoton states H_sH_i and V_sV_i (for example, the residual material birefringence of the optical elements can cause different phase retardations to the H- and V-polarized photons) is stable and is absorbed into 2φ, and the overall phase term is dropped for simplicity. It is known that rotations of the λ/2-wave plate and the λ/4-wave plate in the pump beam path can make $2\varphi=0$ or π to make the Bell states $\Phi^\pm=H_sH_i\pm V_sV_i$ [17]. In addition, rotating a λ/2-wave plate in the signal beam path by 45° allows the other two Bell states $\Psi^\pm=V_sH_i\pm H_sV_i$ to be prepared.

The propagation of a picosecond laser pulse in an optical fiber instantly influences the local material birefringence, changing the photon polarization. This effect is known as polarization switching [9]. In addition to the states just discussed, the third-order nonlinearity of the fiber also allows biphotons to be produced in both the x-polarization state by the $\chi^{(3)}_{xxxx}$ SFWM process and the y-polarization state by the

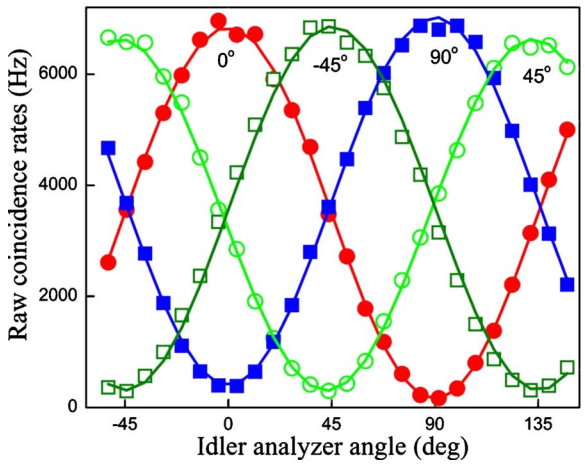

FIG. 2. (Color online) Raw coincidence count rates as a function θ_i for four different values of θ_s $(0°,45°,90°,-45°)$ along with fits to $\sin^2(\theta_i)$ (lines). A 10 s integration time was used for each point. $\lambda_s=689$ nm and $\lambda_i=800$ nm.

$\chi^{(3)}_{xxyy}$ SFWM process [$\chi^{(3)}_{xxyy}\approx(1/3)\chi^{(3)}_{xxxx}$] [9]. The configuration of the fiber Sagnac interferometer allows these spontaneously created photons, with polarization orthogonal to that of the pump (produced from the polarization switching and $\chi^{(3)}_{xxyy}$ SFWM process), to be switched out from the unused port C of the PBS without contaminating the Bell states created at the PBS and output from port D. Those biphoton states produced from the two counterpropagating $\chi^{(3)}_{xxyy}$ SFWM processes also make Bell states $\Phi^+=H_sH_i+V_sV_i$ output from port C. The analysis of those Bell states will be presented elsewhere.

In a previous work [18], we examined the gain spectra of the Raman scattering and SFWM in this PMMF. We measured a 10 THz (≈21 nm) 3 dB bandwidth for the production of biphoton states with high spectral brightness and small background. Based on that measurement, for the current experiment we set the slits in the signal and idler paths to select $\lambda_s=689$ nm and $\lambda_i=800$ nm with $\Delta\lambda=0.9$ nm (0.5 THz), all within the 10 THz band. We measured the quantum-interference fringe visibilities of the Bell state $\Phi^-=H_sH_i-V_sV_i$ at four different angle settings θ_s, for the polarization analyzer in the signal arm: $\theta_s=0°,45°,90°,-45°$. The visibility is defined as $V=(C_{\max}-C_{\min})/(C_{\max}+C_{\min})$, where $C_{\max}$ and $C_{\min}$ are the maximum and minimum coincidence count rates, respectively. The coincidence rates oscillate sinusoidally with the angle of the polarization analyzer (θ_i) in the idler arm as shown in Fig. 2. With a total average pump power of 300 μW, we measured single rates of 120 kHz for the signal and 150 kHz for the idler, and a maximal coincidence rate of 7 kHz at a brightness of 26 kHz nm^{-1} mW^{-1} with a detection efficiency of 0.7% for H polarization and 0.4% for V polarization [consisting of 90% (70%) grating efficiency for H (V) polarization, 93% PBS efficiency, 50% fiber coupling efficiency, 55% interference filter efficiency, detector quantum efficiency (Silicon Avalanche-Photo-Diode), and other system losses]. The visibilities calculated based on the fit parameters are listed in Table I. Without subtracting accidental coincidences, the visibilities are greater than 91% for all four values of θ_s. After subtracting the accidental coincidences, the visibilities are greater than 97%. While the two-photon detection rate of the best down-conversion-based source [17,19] is currently larger than what we have demonstrated with a fiber-based source, the two-photon *brightness* per unit pump power demonstrated for our fiber-based source is among the best values demonstrated for any down-conversion source [20].

TABLE I. Quantum-interference fringe visibility.

θ_s (deg)	Visibility (%) (raw)	Visibility (%) (accidentals subtracted)
0	95.8±1.1	100±1.2
45	91.3±1.0	97.6±1.1
90	91.6±1.1	97.5±1.2
−45	91.3±0.5	97.1±0.6

We also measured the S parameter, a test of nonclassicality defined by the Clauser-Horne-Shimony-Holt form of Bell's inequality [12]. The analyzer settings in the signal arm were $\theta_s=0°,90°,-45°,45°$ and in the idler arm were $\theta_i=-22.5°,67.5°,22.5°,112.5°$, totaling 16 coincidence measurements. Each measurement setting took 10 s to complete, with the resulting S values listed in Table II. In less than 3 minutes for each Bell state, we demonstrated a violation of the classical limit of $S=2$ by more than 20 standard deviations. S was calculated using raw coincidence data with no subtraction of accidentals.

Our two-pass grating configuration allows us to select Bell states at different wavelengths by simply translating slits in the signal and idler paths to different predetermined positions. By moving the slits from previous settings to select $\lambda_s=693$ nm and $\lambda_i=795$ nm, without any additional optical alignment, we immediately obtain the Bell state $\Phi^-=H_sH_i-V_sV_i$ at the new wavelengths. The two-photon coincidence rate remains at the 7 kHz level. The quantum interference fringe visibilities remain above 97% (with accidentals subtracted), as shown in Fig. 3. The measured S parameter of 2.490±0.015 violates the classical limit by 32 standard deviations.

The key characteristics that enabled these advances result from a combination of the microstructure fiber, the Sagnac interferometer, and the achromatic polarization control produced by the fiber twist. The microstructure fiber provides high nonlinearity and dispersion control, allowing high two-photon gain at large detuning where the single-photon background is small [16]. The Sagnac configuration is one of the most stable interferometers because the two counterpropagat-

TABLE II. Measured value of S for all four Bell states.

Bell state	S	Violation (σ)
$H_sH_i+V_sV_i$	2.622±0.016	37
$V_sH_i+H_sV_i$	2.567±0.016	34
$V_sH_i-H_sV_i$	2.321±0.014	22
$H_sH_i-V_sV_i$	2.408±0.015	27

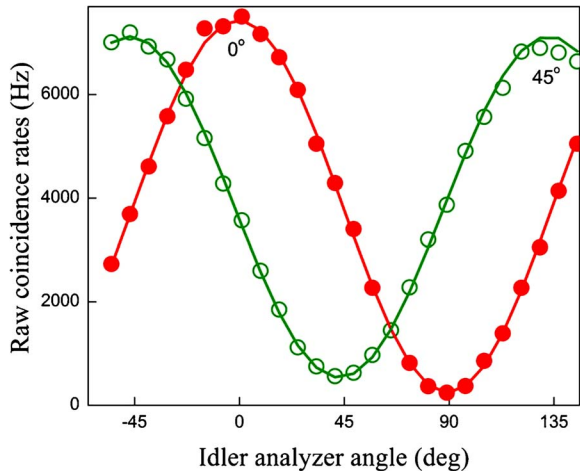

FIG. 3. (Color online) Raw coincidence count rates (dots) as a function of θ_i for two different values of θ_s $(0°, 45°)$ along with fits to $\sin^2(\theta_i)$ (lines). A 10 s integration time was used for each point. λ_s=693 nm and λ_i=795 nm.

ing beams travel identical paths. Lastly, a simple twist of the fiber allows the polarization to be rotated in a wavelength-independent way.

We note that the broad bandwidth of this source would best be exploited by an implementation that uses standard wavelength-division-multiplexing components typical of fiber networks with all their concomitant advantages. In addition to the benefits demonstrated for our source, the gain and dispersion of PMMF can be controlled through design of the fiber structure such as the core, air-hole size, and material nonlinearity, allowing even higher two-photon flux with lower background at wavelengths ranging from uv to infrared.

Although still at an early stage of development, this source is already comparable to its competitors in spectral mode brightness per unit pump power. This bright, phase-stable, easily tunable, broadband-coverage, fiber-based source of polarization-entangled photon pairs should be particularly useful to various quantum-information applications.

ACKNOWLEDGMENTS

This work has been supported in part by the Disruptive Technology Office (DTO) Entangled Photon Source Program, and the Multidisciplinary University Research Initiative Center for Photonic Quantum Information Systems (Army Research Office/DTO Grant No. DAAD19-03-1-0199). M.D.E. acknowledges support from the National Research Council Postdoctoral Research Associateship Program.

[1] C. Cinelli, M. Barbieri, R. Perris, P. Mataloni, and F. De Martini, Phys. Rev. Lett. **95**, 240405 (2005).
[2] H. Takesue, E. Diamanti, T. Honjo, C. Langrock, M. M. Fejer, K. Inoue, and Y. Yamamoto, New J. Phys. **7**, 232 (2005).
[3] C. H. Bennett, G. Brassard, C. Crepeau, R. Jozsa, A. Peres, and W. K. Wootters, Phys. Rev. Lett. **70**, 1895 (1993); D. Boumeester, J. W. Pan, K. Mattle, M. Eibl, H. Weinfurter, and A. Zeilinger, Nature (London) **390**, 575 (1997).
[4] A. K. Ekert, Phys. Rev. Lett. **67**, 661 (1991).
[5] P. G. Kwiat, E. Waks, A. G. White, I. Appelbaum, and P. H. Eberhard, Phys. Rev. A **60**, R773 (1999); J. F. Hodelin, G. Khoury, and D. Bouwmeester, *ibid.* **74**, 013802 (2006).
[6] L. J. Wang, C. K. Hong, and S. R. Friberg, J. Opt. B: Quantum Semiclassical Opt. **3**, 346 (2001).
[7] H. Takesue and K. Inoue, Phys. Rev. A **70**, 031802(R) (2004).
[8] X. Li, P. L. Voss, J. E. Sharping, and P. Kumar, Phys. Rev. Lett. **94**, 053601 (2005).
[9] G. P. Agrawal, *Nonlinear Fiber Optics*, 2nd ed. (Academic, New York, 1995).
[10] K. F. Lee, J. Chen, C. Liang, X. Li, P. L. Voss, and P. Kumar, Opt. Lett. **31**, 1905 (2006).
[11] P. L. Voss and P. Kumar, J. Opt. B: Quantum Semiclassical Opt. **6**, 762 (2004).
[12] J. F. Clauser, M. A. Horne, A. Shimony, and R. A. Holt, Phys. Rev. Lett. **23**, 880 (1970).
[13] J. C. Knight, T. A. Birks, P. St. J. Russell, and D. M. Atkin, Opt. Lett. **21**, 1547 (1996).
[14] T. A. Birks, J. C. Knight, and P. St. J. Russell, Opt. Lett. **22**, 961 (1997).
[15] T. M. Monro, D. J. Richardson, N. G. R. Broderick, and P. J. Bennett, J. Lightwave Technol. **17**, 1093 (1999).
[16] J. Fan, A. Migdall, and L. J. Wang, Opt. Lett. **30**, 3368 (2005).
[17] T. Kim, M. Fiorentino, and F. N. C. Wong, Phys. Rev. A **73**, 012316 (2006); F. N. C. Wong, J. H. Shapiro, and T. Kim, Laser Phys. **16**, 1517 (2006).
[18] J. Fan and A. Migdall, Opt. Express **15**, 2915 (2007).
[19] J. Altepeter, E. Jeffrey, and P. G. Kwiat, Opt. Express **13**, 8951 (2005).
[20] See, for example, the 5 kHz nm^{-1} mW^{-1} brightness, with a two-photon coincidence rate of 16 kHz in a 1 nm collection bandwidth and 3.3 mW pump power, obtained in a type-II down-conversion system using periodically poled $KTiOPO_4$ [17]; and the 0.3 kHz nm^{-1} mW^{-1} result using type-I down-conversion with two β-barium borate crystals, with a two-photon coincidence rate of 2 MHz in a 25 nm collection bandwidth and 280 mW pump power [19]. Recently, we became aware of the detection of two-photon coincidence at a rate of 273 kHz nm^{-1} mw^{-1} via a down-conversion process in a PPKTP bulk crystal reported by Fedrizzi *et al.*, e-print arXiv:0706.2877v1.